Article

Evaluation of NOx Reduction Effect and Impact on Asphalt Pavement of Surface Treatment Technology including TiO$_2$ and Asphalt Rejuvenator

Jong-Won Lee and Cheolmin Baek *

Department of Highway and Transportation Research, Korea Institute of Civil Engineering and Building Technology, 283 Goyangdae-ro, Ilsanseo-gu, Goyang-si 10223, Korea; asca28@kict.re.kr
* Correspondence: cmbaek@kict.re.kr; Tel.: +82-31-910-0613

Abstract: Nitrogen oxide (NOx), emitted at the highest rate among automobile exhaust gases, is the main cause of air pollution, and various construction technologies are being developed to reduce NOx emissions. In this study, the NOx reduction effect of surface treatment technology for road pavements, and the effect of the photocatalytic reaction on asphalt pavements, were evaluated using a photocatalyst. Three types of titanium dioxide (TiO$_2$) were used as photocatalysts, and an asphalt rejuvenator used to recover aged asphalt was applied as a surface treatment agent. To evaluate the NOx reduction effect, a test device capable of testing large-sized specimens was manufactured and compared with the ISO method, which only allowed the testing of small specimens. In addition, the effect of TiO$_2$ and the asphalt rejuvenator on the asphalt mixture was analyzed through chemical analysis. The test results of the newly manufactured mixed-tank photo reactor showed the same trend as the ISO test results concerning the evaluation of its NOx removal performance. As a result of the performance evaluation of the surface treatment using TiO$_2$, the NO removal rate was up to 7.83% when Anatase-type TiO$_2$ with excellent light efficiency was applied. In addition, when the rejuvenator was used, the oxidation of asphalt, caused by the photoreaction of TiO$_2$, was reduced.

Keywords: titanium dioxide; asphalt surface treatment; nitrogen oxide; photocatalytic reaction

1. Introduction

Recently, air pollution has negatively affected various social, environmental, and industrial aspects. In particular, in cities with a high population density, roadside air pollution caused by automobile exhaust gas is emerging as a serious environmental problem [1,2]. Nitrogen oxide (NOx), which is emitted in the highest quantities from automobiles, is known to be harmful not only to the air environment but also to human health. It is also well known as a harmful gas component that causes diseases of the respiratory system as well as photochemical smog and acid rain [3]. To solve this problem, research has been conducted to reduce exhaust gas emissions from automobiles, and solutions such as the use of clean fuel with fewer pollutants, and the installation of automobile exhaust system purification equipment, have been proposed. However, owing to the continuous increase in the number of vehicles operated, the emission of nitrogen oxides continues to steadily increase, and various alternative technologies for reducing NOx emissions are required.

Photocatalysts are used to purify air pollution caused by NOx, and titanium dioxide (TiO$_2$) is known to be the most effective material among various photocatalysts [4–7]. TiO$_2$ has better chemical stability than other photocatalysts and is not corroded by most acids, bases, and organic solvents, so it is actively used in various fields [8–12]. The application of TiO$_2$ in the construction field is being studied for application to large surface areas, such as the exterior of buildings and road pavements [13–16]. In the case of road pavements applied with TiO$_2$, as shown in Figure 1, electrons (e$^-$) and holes (h$^+$) are formed due to a photocatalytic reaction when exposed to ultraviolet (UV) light. The generated electrons

and holes react with O_2 and H_2O in the air, respectively, to generate active oxygen of superoxide anion (O_2^-) and hydroxyl radical (OH^-) on the surface of TiO_2, thereby decomposing NOx into nitrate (NO_3^-). This nitrate is washed away by rain in the form of an aqueous solution of nitric acid (HNO_3). This complex reaction mechanism is used to reduce NOx in the atmosphere and remove NO_3 through biological denitrification in the groundwater zone [17,18].
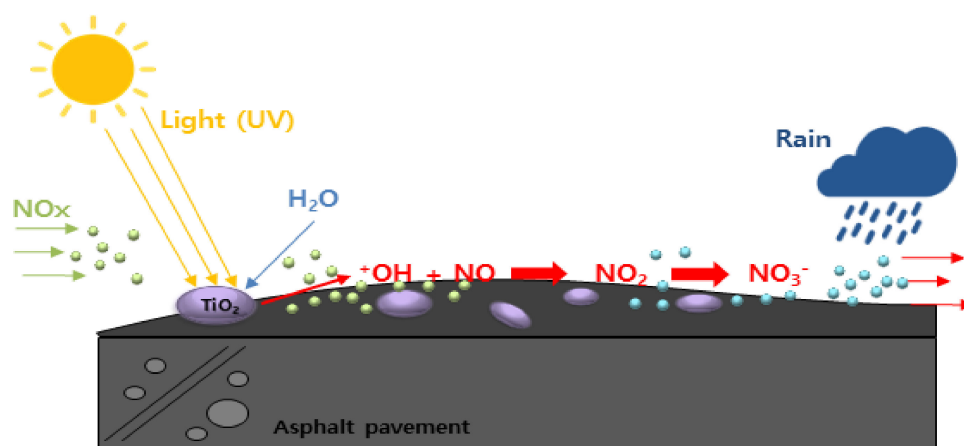
Figure 1. Image of NOx decomposition by TiO_2.

There are two possible methods for applying TiO_2 to the asphalt pavements that occupy the majority of urban roads. One method is to produce an asphalt mixture by adding TiO_2 powder during the mix design, and the other is to coat the existing asphalt pavement surface with TiO_2 mixed with liquid adhesive [19–21]. The method of directly mixing TiO_2 with the asphalt mixture is not economical because exposure to UV is limited, and a large amount of photocatalyst is used [22–24]. To overcome these shortcomings, various methods of coating the surface of an asphalt pavement with TiO_2 solution have been recently attempted. These include: mixing TiO_2 with an aqueous solution, or asphalt binder, and then spraying it on the road surface; using TiO_2 as an asphalt modifier; coating TiO_2 on waste rubber and then spraying the rubber mixture on the pavement surface; and coating the road surface with an asphalt emulsion mixed with TiO_2 [25–31]. However, these methods are complicated and limited in manufacturing and construction and do not provide sufficient durability and NOx removal efficiency for field applications. In addition, because TiO_2 uses UV as an energy source, it may promote the aging and oxidation of binders used for coatings and existing asphalt pavements [32,33].

Meanwhile, one of the main challenges in testing construction materials (paint, cement, tile, asphalt, concrete, etc.) with TIO_2 is finding a way to determine the NOx decomposition effect. The most popular methods are the ISO standard, which uses a bed flow photoreactor, and the UNI standard, which adapts a mixed tank photoreactor. In addition, many reactors with various configurations have been proposed and published [34,35]. An acrylic flow reactor equipped with a Pyrex window [36], quartz reactor [37], fixed bed reactor [38], glass holder plate reactor [39], continuous stirred tank reactor (CSTR), and plug flow reactor (PFR) were used to analyze the NOx decomposition effect of the photocatalyst [34]. The problem with these experiments is that a discrepancy between the laboratory results and the field performance exists because the sample size is very small compared to the actual size applied to the field [40]. Therefore, in this study, a reactor capable of accommodating large specimens that can simulate the actual site was developed, and the NOx decomposition effect of pavement surface treatment materials, including TiO_2, was evaluated using this reactor. In this study, the NOx decomposition effect of asphalt surface treatment technology, including TiO_2 and asphalt rejuvenator, was evaluated. Two types of test equipment were prepared: the ISO standard test with bed flow photoreactors using small specimens and a newly developed mixed tank photoreactor using a large specimen. First, the differences

between the two pieces of equipment were compared and analyzed using various types of TiO_2 powder. Then, the NOx decomposition effect of the large specimen, surface treated with TiO_2 and the asphalt rejuvenator, was evaluated using mixed tank photoreactors. Finally, the effect of TiO_2 and the asphalt rejuvenator on the asphalt mixture was analyzed through FT-IR and SARA analyses.

2. Materials and Test Methods

2.1. Materials

2.1.1. Photocatalyst

In this study, the photocatalyst used as the surface treatment agent was TiO_2, and three TiO_2 types with different specific surface areas were used to compare the differences in the NOx decomposition effect. The crystal structures of TiO_2 are anatase-type, with excellent light efficiency, and a combination of anatase and rutile, with an average particle size of 20–30 nm. The properties of the TiO_2 used are listed in Table 1.

Table 1. Physical properties of TiO_2.

Physical Properties	Type-1	Type-2	Type-3
Constituent	Anatase (80%) + Rutile (20%)	Anatase (100%)	Anatase (100%)
Purity (%)	<99	<99	<94
Surface area (m²/g)	35–65	60–70	78
Apparent density (g/mL)	0.1–0.18	0.45	0.6
Particle size (nm)	20–30	20–30	20–30

2.1.2. Surface Treatment Agent

An asphalt rejuvenator, which is mainly used for the preventive maintenance of aged asphalt pavement, was used as a surface treatment agent. It is a transparent, colorless liquid material manufactured mainly with vegetable raw materials and styrene-butadiene-copolymer (SBC) additives. It is applied directly to asphalt pavements using a spray-type spreader. It penetrates to a depth of approximately 5 to 10 mm inside the asphalt pavement and restores the viscosity of the asphalt binder to improve the bonding strength with aggregates and increase elasticity, thereby strengthening the durability of the asphalt pavement. Tables 2 and 3 show the physical and chemical properties of the asphalt rejuvenator.

Table 2. Physical properties of the asphalt rejuvenator.

Properties	Results		Test Method
Specific gravity	0.85~0.95		ASTM D-1298
Water	1% Max		ASTM D-95
	Temp. (°C)	Distillate (%)	
Distillation residue	170	0–40	ASTM D-158
	270	0–5	
	300	0–5	
Viscosity	10–50 Sec @ 122 °F		ASTM D 88
Flash point	110 °F		
Percent volatile	5–40		

Table 3. Chemical properties of the asphalt rejuvenator.

Chemical Compositions (%)	
D-Limonene	75
Soybean oil, methyl ester	20
Reactive polymer	5

2.1.3. Materials for Asphalt Concrete Specimen

For the asphalt concrete specimen used in this study, the materials and asphalt mixture mix design were in accordance with the standards generally used for the surface layer of asphalt pavement in South Korea. An asphalt binder of PG 64–22 grade and granite crushed stone aggregate with a flat and elongated particle ratio of 10% or less were utilized. Tables 4 and 5 detail the characteristics of the asphalt binder and aggregate used in this study.

Table 4. Specifications of the asphalt binder.

Properties	Results	Test Method
Penetration (1/10 mm)	71	ASTM D 5
Density (g/cm^3)	1.036	ASTM D 70
Flash point (°C)	338	ASTM D 95
Softening point (°C)	44	ASTM D 158
Ductility (15 °C)	150+	ASTM D 113
Solubility in trichloroethylene (%)	99.78	ASTM D 2042
Mass change after thin-film oven test (%)	−0.02	ASTM D 2872
Retained penetration after thin-film oven test (%)	69.0	ASTM D 2872

Table 5. Properties of the aggregate.

Nominal Maximum Aggregate Size (mm)	Density (g/cm^3)	Absorption (%)	Abrasion (%)	Flat or Elongated Particle Ratio (wt.%)
20	2.72	0.52	13.8	7.5

2.2. Experimental Methods

2.2.1. Specimen Fabrication

For the specimen used in the experiment, a slab specimen of dimensions 300 mm × 300 mm × 50 mm was fabricated with 4% air voids using a roller press compactor. The produced specimen was cured at room temperature for 24 h and then stored in an environmental chamber at 25 °C for 6 h before being used for testing. For the surface treatment solution, TiO$_2$ was added to the asphalt rejuvenator by 5% of the weight of the rejuvenator and then mixed for 30 min with a high-speed stirrer. The mixed surface treatment solution was sprayed on the prepared specimen at a rate of 0.4 kg/m^2, and the test was carried out after curing at 25 °C for 1 h. Figure 2 show the mechanism by which the surface treatment solution acts on the specimen, and Figure 3 is the final surface treated specimen.

2.3. Photo Reactors Test

To evaluate the NOx removal performance according to the type of reactor, photoreactors were designed, as shown in Figure 4. Two evaluation systems were established based on this design. The bed flow photoreactor type tester complying with ISO 22197-1 (2007) is shown in Figure 5. The evaluation system manufactured using the mixed tank photoreactor method is shown in Figure 6. A calibrator was installed to control the concentration of NOx flowing into the reactor, and a hydraulic system and valve device were configured to control the NOx inflow. To check the inlet NOx concentration, the T-connection of the photoreactor was connected to the NOx analyzer. A gas mixture of NOx and zero air entered and filled the photoreactor at a controlled humidity, flow, and NOx concentration. Before entering the photoreactor, the inlet jet stream continued through the humidifier to control humidity. The size of the bed flow photoreactor was 100 × 50 × 10 mm, whereas the size of the photoreactor of the mixed tank was 500 × 500 × 500 mm. Both methods were hermetically sealed to prevent the inflow of outside air and to maintain a controlled environment for the sample. A UV lamp was installed on the upper part of the photoreactor

to simulate ultraviolet light for the photoactivation reaction. The experiment was carried out to measure the amount of NOx reduction by installing a test specimen prepared in each reactor and setting the concentration of NOx input into the reactor to 1.00 ppm. In the state where NOx continuously flowed through the reactor, the light source of the UV lamp was irradiated at 10 W/m^2 for more than 5 h, and the change in NOx concentration according to the light source was measured in units of 1 min. All tests were performed at a temperature of $25 \pm 2 \degree C$ and a humidity of $45 \pm 5\%$.
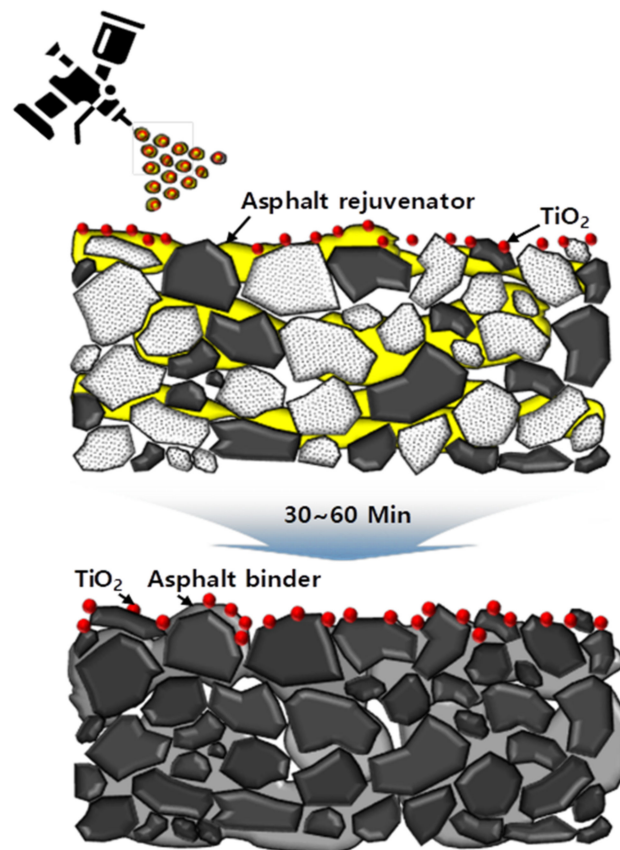

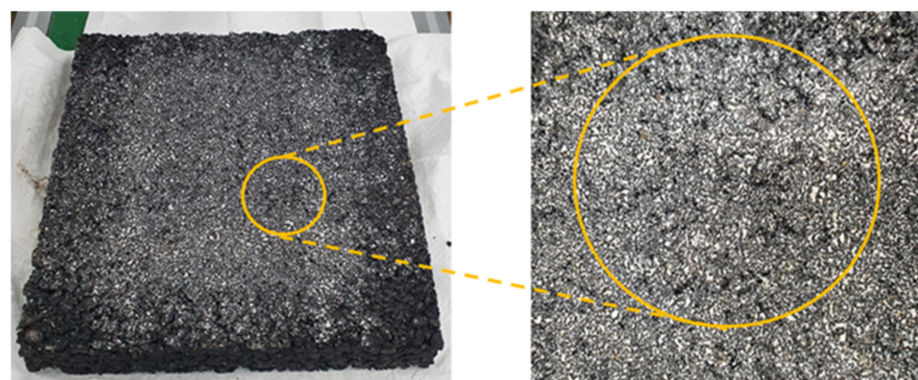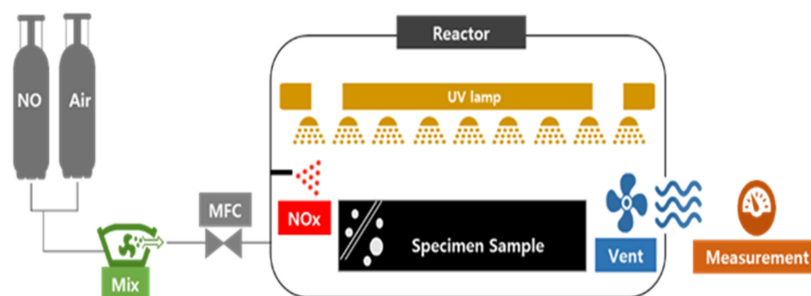**Figure 2.** Coating mechanism of TiO_2.

Figure 3. Images of the surface treated specimens.

Figure 4. Schematic diagram of the NOx analysis system.

Figure 5. Image of the NOx analysis system (bed flow photo reactors).

Figure 6. Image of the NOx analysis system (mixed tank photo reactors).

2.4. FT-IR Spectroscopy Analysis

FT-IR (spectroscopy spectrum 100, PerkinElmer Inc., Seoul, Korea) of the attenuated total reflection method was used to confirm the changes in the molecular structure and functional groups of asphalt before and after UV irradiation. The sample was kept constant by force gauge 148, and the average value measured by scanning each sample 16 times was used. The measured wavenumber ranged from 4000 to 650 cm^{-1}, and the spectrum is shown as an absorbance graph.

2.5. SARA Analysis

SARA analysis was performed to confirm asphalt aging and oxidation before and after UV irradiation. One microliter of sample dissolved in DCM solvent at 1% (w/v) was loaded onto a rod-shaped silica rod for TLC development, and the analysis was performed by sequentially developing it in a prepared developing solvent (hexane, toluene,

and DCM/methanol (95:5)). The content of each component was analyzed using the FID detector of the IATROSCAN MK-6 (Iatron Lab. Inc., Tokyo, Japan) and a TLC-FID analyzer. The FID measurement conditions were air 2.0 L/min, hydrogen 160 mL/min, and scan speed 30 s/scan.

3. Experimental Results and Analysis

3.1. Evaluation of NOx Removal Performance by Reactor Type

3.1.1. Bed Flow Photo Reactors Test Result

To verify the NOx removal efficiency of the bed flow photoreactors (ISO standard) and mixed tank photoreactors, the NOx removal performance of each reactor was evaluated using TiO_2 powder. Bed flow photoreactor tests were performed at a flow rate of 1 L/min, UV intensity of 10 W/m^2, temperature of 25 $\pm$ 5 °C, and humidity of 45 $\pm$ 5%. Figure 7 show the change in NOx concentration in the bed flow photoreactor experiments for TiO_2. Before turning on the UV light, the initial NOx concentration in the chamber was equilibrated to 1 ppm. After turning on the UV light, the concentrations of NOx and NO were reduced, and NO_2 was produced owing to the oxidation of NO. After 5 h of experimentation, the UV light was turned off, and the concentration showed a tendency to increase again. Table 6 show the NO removal efficiencies by TiO_2 type. In the case of Type-1, the NO removal rate was 26.06%, the Type-2 NO removal efficiency was 18.52%, and the Type-3 NO removal efficiency was 21.82%.
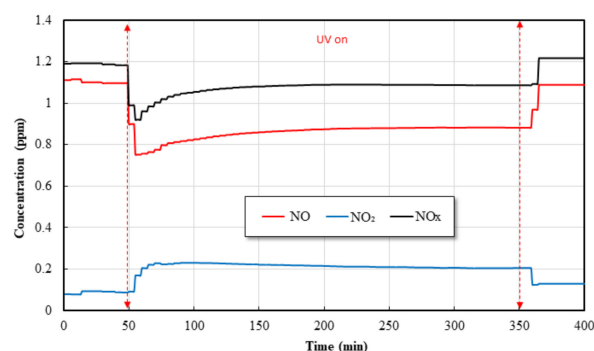

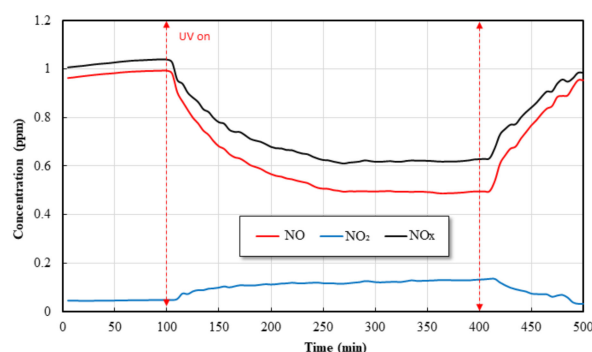**Figure 7.** Variation of NOx concentrations during the bed flow photo reactor experiment.

Table 6. NO reduction and reduction efficiency of bed flow photo reactors.

Test ID	Total NO (umol)	Total Removed No (umol)	Total Removed No (%)
Type-1	13.59	3.59	26.06
Type-2	13.55	2.51	18.52
Type-3	13.71	2.99	21.82

3.1.2. Mixed Tank Photo Reactor Test Result

A mixed tank photoreactor was operated at a flow rate of 3 L/min, UV intensity of 10 W/m^2, temperature of 25 $\pm$ 5 °C, and humidity of 45 $\pm$ 5%. Figure 8 show the change in NOx concentration in the mixed-tank photo reactor experiment for TiO_2. As the reactor is larger than the bed flow photoreactor, the UV light was turned on after maintaining a stable state of NOx concentration in the reactor for approximately 100 min. Before turning on the UV light, the initial concentration in the chamber was equilibrated to 1 ppm. As with the bed flow photoreactor method, the concentrations of NOx and NO were reduced after turning on the UV light, and NO_2 was generated due to NO oxidation. After the experiment was performed for 5 h, the UV light was turned off, and after that, it had a slight equilibrium state for 10 min before showing a tendency to increase again. In the case of the mixed tank photoreactor method, which has a larger reactor size than the bed flow photoreactor, the reaction does not occur immediately when the UV light is turned on, and

the NOx and NO concentrations gradually decrease until 2 h and 30 min before remaining in a parallel state. Table 7 show the NO removal efficiencies by TiO_2 type. In the case of Type-1, the NO removal rate was 43.66%, the Type-2 NO removal efficiency was 31.41%, and the Type-3 NO removal efficiency was 41.65%.

Figure 8. Variation of NOx concentrations during the mixed tank photo reactor experiment.

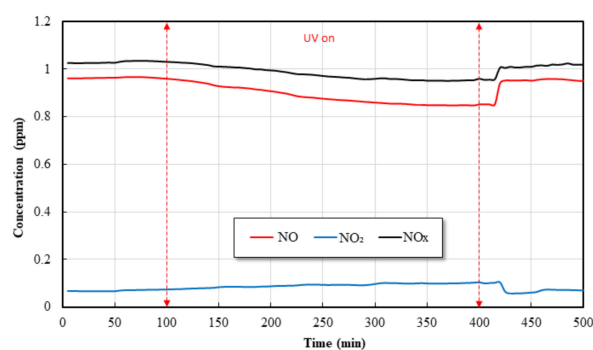**Table 7.** NO reduction and reduction efficiency of mixed tank photo reactors.

Test ID	Total NO (umol)	Total Removed NO (umol)	Total Removed NO (%)
Type-1	38.74	16.92	43.66
Type-2	37.62	11.82	31.41
Type-3	38.27	15.94	41.65

In the NOx removal performance evaluation experiment of each reactor, the NOx removal rate of the three TiO_2 types showed a similar trend, but the NOx reduction rate of the mixed tank photoreactor method was higher. This is because the amount of TiO_2 used in the experiment was the same, but the NOx and TiO_2 contact surfaces were much larger in the mixed tank photoreactor. Only specimens of limited size can be applied to bed flow photoreactors, whereas mixed tank photoreactors increase the contact surface with NOx because the size of the reactor is larger even if the same amount of TiO_2 is used. Therefore, the amount of TiO_2 that can react with NOx is higher than that of bed flow photoreactors. It was found that the NOx reduction effect in the mixed tank photoreactor increased by 65%–90%. Through the mixed tank photoreactor, construction materials and secondary products that could not be tested in the existing bed flow photoreactors (ISO standard) could be evaluated without reprocessing the specimen size, and the performance deviation from the field is expected to be reduced.

3.2. Evaluation of NOx Removal Performance of the TiO_2 Surface Treated Asphalt Specimens

To evaluate the efficiency of the NOx removal performance of TiO_2 surface treated asphalt specimens, an experiment was conducted using a mixed tank photoreactor. The specimen used for surface treatment was an asphalt specimen manufactured in the form of a slab with a width of 300 mm, length of 300 mm, and thickness of 50 mm. A mixed tank photoreactor test was performed at a flow rate of 3 L/min, UV intensity of 10 W/m^2, temperature of 25 ± 5 °C, and humidity of 45 ± 5%. Similar to the experimental results in Section 3.1, the NOx and NO concentrations gradually decreased until 2 h and 30 min after the UV light was turned on, and then, a parallel state was maintained. Figure 9 show the change in NOx concentration in the mixed tank photoreactor experiment on the surface treated asphalt specimen, and Table 8 show the experimental results according to the type of TiO_2.

Figure 9. Variation of NOx concentrations on the surface treated asphalt specimen during the mixed tank photo reactor experiment.

Table 8. NO reduction and reduction efficiency on the surface treated asphalt specimen of mixed tank photo reactors.

Test ID	Total NO (umol)	Total Removed NO (umol)	Total Removed NO (%)
Type-1	37.44	0.95	2.54
Type-2	37.07	2.20	5.94
Type-3	37.54	2.94	7.83

As a result of the experiment, each TiO_2 surface treated specimen exhibited a photocatalytic reaction. The NO removal efficiencies of the surface treated asphalt specimens were 2.54% for Type-1, 5.94% for Type-2, and 7.83% for Type-3. Surface treated specimens exhibited a tendency to significantly decrease NOx removal performance compared to the TiO_2 powder test result in Section 3.1, which can be explained by two reasons.

The first is the reduction in the specific surface area of TiO_2. In the case of TiO_2 in powder form in the previous experiment, all surfaces of TiO_2 can undergo photocatalytic reactions. However, in the case of TiO_2 mixed with a surface treatment agent, the viscosity of the asphalt binder in the specimen is restored by the rejuvenator, and the TiO_2 fixed to the asphalt binder does not photocatalytically react. As the specific surface area that can be reacted to becomes smaller than that of the powder, the ability to reduce NOx decreases [41,42]. The second is the particle change due to the aggregation of TiO_2, as shown in Figure 10. Nano-sized TiO_2 has the property of aggregating by interparticle attraction due to its negative charge action. Similar to the first reason, the specific surface area of TiO_2 capable of a photocatalytic reaction was reduced. TiO_2 in the agglomerated state forms flocs, and the particle size and sedimentation rate are relatively increased [43]. These TiO_2 are precipitated in the asphalt binder, whose viscosity is restored and softened, preventing the photocatalytic reaction. Therefore, it is estimated that the NO reduction rate of the surface treated asphalt specimen is lower than that of TiO_2 in powder form.
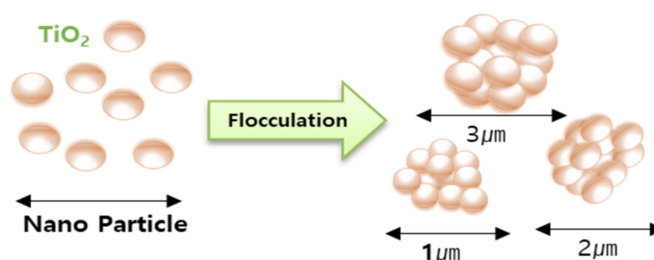
Figure 10. Flocculation of nano particle TiO_2.

3.3. Asphalt Aging Evaluation by UV

3.3.1. FT-IR Spectroscopy Analysis

TiO_2 is known to accelerate the oxidation and aging of asphalt because it uses UV as an energy source. Therefore, a UV aging test was conducted to determine the effect of the surface treatment agent produced in this study on asphalt aging. The UV aging experiment was repeated 10 times for 5 h each, and the total time of exposure to UV was 50 h so that the asphalt was sufficiently aged by UV. The UV aging test was conducted on three specimens: general asphalt, asphalt mixed with TiO_2, and asphalt mixed with TiO_2 and the rejuvenator. The TiO_2 used for the specimen preparation was type-1. After UV aging, the asphalt binder was extracted and analyzed using FT-IR to confirm the changes in the molecular structure and functional groups of the asphalt. The analysis results are shown in Figures 11 and 12.
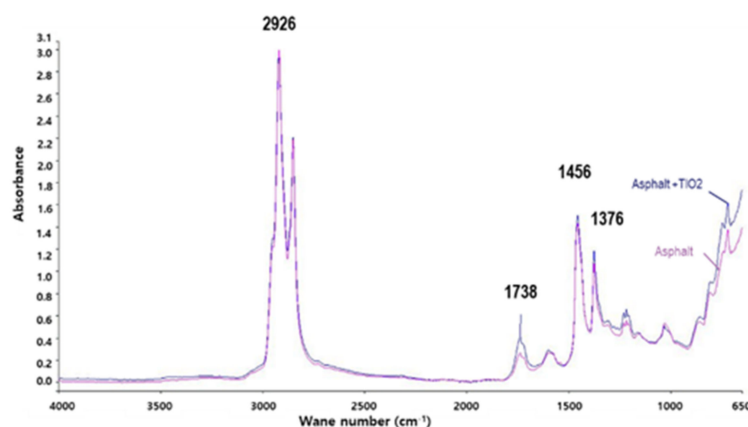

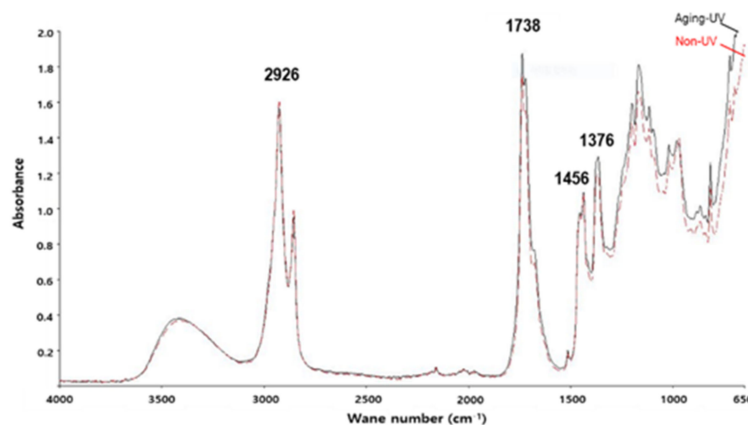**Figure 11.** FT-IR spectrum of asphalt and asphalt with TiO_2.

Figure 12. FT-IR spectrum of Asphalt mixed with surface treatment agent.

Figure 11 show the results of the FT-IR experiments of asphalt and TiO_2 mixed asphalt after UV aging. The peak at 2926 cm^{-1} corresponds to the sp^3 C-H stretching vibration of saturated hydrocarbons, the peak at 1456 cm^{-1} corresponds to the -CH$_2$ bending vibration, and the peak at 1376 cm^{-1} corresponds to the -CH$_3$ bending vibration. The peak at 1738 cm^{-1} corresponds to the C=O stretching vibration of the ester carboxyl functional group (COO) and is used as an index to predict the degree of oxidation of asphalt [44].

A comparison of the intensity of the peak at 1738 cm^{-1} by aligning the peaks at 2926 cm^{-1} in both spectra with the same intensity revealed that the intensity of the peak at 1738 cm^{-1} of the asphalt containing TiO_2 compared to the asphalt without TiO_2 increased by approximately 30%. This means that the asphalt mixed with TiO_2 is highly affected by photooxidation, and the asphalt in the area in direct contact with TiO_2 is partially and

rapidly oxidized. Therefore, TiO_2 in asphalt is expected to accelerate the aging of asphalt owing to oxidation by UV.

Figure 12 show the FT-IR test results of asphalt samples mixed with TiO_2 and the rejuvenator. The peak at 3000 cm^{-1} corresponds to the -OH stretching vibration, which is an absorption peak that appears mainly in asphalt-containing polymers [45]. Since the peak at 1738 cm^{-1} is much larger than that of general asphalt, it seems that the rejuvenator contains an SBC polymer additive and a component with an ester functional group.

The peak change before and after the UV aging test showed that the intensity of the C=O stretching vibration at 1738 cm^{-1} increased by 10% based on the peaks at 2926 and 1456 cm^{-1}. Therefore, it was found that oxidation was less advanced when the rejuvenator was mixed than when only TiO_2 was mixed with asphalt.

3.3.2. SARA Analysis Result

In general, changes in the SARA components occur in asphalt owing to aging. At the beginning of the aging reaction, the aromatic hydrocarbon component (aromatics, Ar) increased as the aliphatic saturated hydrocarbon component (saturates, Sa) decreased, and the asphaltene component (As) increased as the petroleum resin component (Resin, Re) decreased. Thereafter, as a two-step change, the Sa component maintained a constant content without further reduction, the Re component increased as the Ar component decreased, and As continuously increased. As asphalt aging by UV continued, the contents of Sa and Ar decreased and the contents of Re and As increased, leading to an increase in the brittleness of asphalt. This resulted in relatively reduced ductility, which ultimately exceeded the fracture toughness and caused cracks [46,47].

The results of SARA analysis through the UV aging experiment are shown in Tables 9–11. As a result of the experiment, we found that the asphalt containing TiO_2 exhibited reduced Sa and Ar content and increased Re and As content compared to general asphalt, indicating that UV-induced aging was accelerated. However, in the case of asphalt mixed with TiO_2 and the rejuvenator, the difference in the SARA components before and after the UV aging test was not significant. Therefore, the rejuvenator is effective in preventing UV aging caused by TiO_2.

Table 9. SARA analysis result of asphalt.

Constituent	Before UV Irradiation	After UV Irradiation
Asphaltene	14.6	50.1
Resin	10.2	4.4
Aromatic	48.2	33.1
Saturate	29.4	11.4

Table 10. SARA analysis result of asphalts and asphalts with TiO_2.

Constituent	Before UV Irradiation	After UV Irradiation
Asphaltene	16.8	35.6
Resin	12.1	37.4
Aromatic	44.8	22.9
Saturate	29.2	4.1

Table 11. SARA analysis result of asphalt mixed with surface treatment agent.

Constituent	Before UV Irradiation	After UV Irradiation
Asphaltene	16.8	19.3
Resin	12.1	11.4
Aromatic	44.8	42.3
Saturate	29.2	27

4. Conclusions

In this study, to verify the NOx decomposition effect of the surface treatment agent applied with TiO_2 and an asphalt rejuvenator, bed flow photoreactors and mixed tank photoreactors were fabricated and tested. In addition, the effects of the TiO_2 and asphalt rejuvenator used as surface treatment agents on asphalt aging were evaluated. The results of this study are as follows:

The mixed tank photoreactor method showed the same trend as the bed flow photoreactor method in terms of the evaluation of the NOx removal performance of the photocatalyst powder despite the difference in test specimen size. Therefore, the mixed tank photoreactor test method can be used to more clearly evaluate the performance of photocatalyst-applied construction materials without reprocessing the sample by replacing the ISO standard test, which was only possible with a limited sample size.

As a result of the evaluation of the NOx removal performance of the surface treatment agent, including TiO_2 and the rejuvenator, the NO removal rate was 2.54–7.83%, depending on the type of TiO_2. This could be caused by a reduction in the specific surface area due to agglomeration and the precipitation of TiO_2 powder when the surface treatment agent was attached to the asphalt specimen.

As a result of FT-IR and SARA analysis, it was found that the asphalt mixed with TiO_2 progressed the oxidation of the asphalt by about 30% under the influence of photooxidation. However, when the rejuvenator, a surface treatment agent, was used together with TiO_2, the oxidation of asphalt progresses only about 10%, and the aging of asphalt due to photooxidation was relatively reduced.

The NOx decomposition effect of TiO_2 using the mixed tank photo reactor presented in this study was conducted using only TiO_2 powder and asphalt surface treatment technology. Therefore, it has been judged that it is necessary to compare these results with the existing ISO test method through additional construction material tests.

References

1. Kan, H.; London, S.J.; Chen, G.; Zhang, Y.; Song, G.; Zhao, N.; Jiang, L.; Chen, B. Season, sex, age, and education as modifiers of the effects of outdoor air pollution on daily mortality in Shanghai, China: The Public Health and Air Pollution in Asia (PAPA) study. *Environ. Health Perspect.* **2008**, *116*, 1183–1188. [CrossRef] [PubMed]
2. Chen, B.; Hong, C.; Kan, H. Exposures and health outcomes from outdoor air pollutants in China. *Toxicology* **2004**, *198*, 291–300. [CrossRef] [PubMed]
3. Hong, S.J.; Lee, S.W. An Experimental Study for the Construction of Photocatalytic Method Concrete Road Structure. *J. Korean Soc. Road Eng.* **2013**, *15*, 1–9. [CrossRef]
4. Fujishima, A.; Rao, T.; Tryk, D.A. Titanium dioxide photocatalysis. *J. Photochem. Photobiol. C Photochem. Rev.* **2017**, *1*, 5525. [CrossRef]
5. Henderson, M.A. A surface science perspective on TiO_2 photocatalysis. *Surf. Sci. Rep.* **2011**, *66*, 185–297. [CrossRef]
6. Guo, M.-Z.; Ling, T.-C.; Poon, C.-S. TiO_2-based self-compacting glass mortar: Comparison of photocatalytic nitrogen oxide removal and bacteria inactivation. *Build. Environ.* **2012**, *53*, 1–6. [CrossRef]

7. Guo, M.-Z.; Ling, T.-C.; Poon, C.-S. Nano-TiO$_2$-based architectural mortar for NO removal and bacteria inactivation: Influence of coating and weathering conditions. *Cem. Concr. Compos.* **2013**, *36*, 101–108. [CrossRef]

8. Jameel, Z.N.; Haider, A.J.; Taha, S.Y.; Gangopadhyay, S.; Bok, S. Evaluation of hybrid sol-gel incorporated with nanoparticles as nano paint. *AIP Conf. Proc.* **2016**, *1758*, 20001.

9. Haider, A.J.; Materials, A.; Materials, A. Synthesis and Characterization of TiO$_2$ Nanoparticles via Sol- Gel Method by Pulse Laser Ablation. *Eng. Technol. J.* **2015**, *33*, 761–771.

10. Sirimahachai, U.; Phongpaichit, S.; Wongnawa, S. Evaluation of bactericidal activity of TiO$_2$ photocatalysts: A comparative study of laboratory-made and commercial TiO$_2$ samples. *Songklanakarin J. Sci. Technol.* **2009**, *31*, 517–525.

11. Qi, M.; Yang, D.; Zhang, J.; Ai, H.J. Preparation and Characterization of Zn-Containing Hydroxyapatite/TiO$_2$ Composite Coatings on Ti Alloys. *Trans. Tech. Publ.* **2011**, *685*, 367–370.

12. Balbuena, J.; Sánchez, L.; Cruz-Yusta, M. Use of Steel Industry Wastes for the Preparation of Self-Cleaning Mortars. *Materials* **2019**, *12*, 621. [CrossRef]

13. Poon, C.S.; Cheung, E. NO removal efficiency of photocatalytic paving blocks prepared with recycled materials. *Constr. Build. Mater.* **2007**, *21*, 1746–1753. [CrossRef]

14. Chen, J.; Poon, C. Photocatalytic construction and building materials: From fundamentals to applications. *Build. Environ.* **2009**, *44*, 1899–1906. [CrossRef]

15. Chen, J.; Poon, C.S. Photocatalytic activity of titanium dioxide modified concrete materials—Influence of utilizing recycled glass cullets as aggregates. *J. Environ. Manag.* **2009**, *90*, 3436–3442. [CrossRef]

16. Guo, M.Z.; Poon, C.S. Photocatalytic NO removal of concrete surface layers intermixed with TiO$_2$. *Build. Environ.* **2013**, *70*, 102–109. [CrossRef]

17. Verdier, T.; Coutand, M.; Bertron, A.; Roques, C. Antibacterial activity of TiO$_2$ photocatalyst alone or in coatings on *E. coli*: The influence of methodological aspects. *Coatings* **2014**, *4*, 670–686. [CrossRef]

18. Ba-Abbad, M.M.; Kadhum, A.A.H.; Mohamad, A.B.; Takriff, M.S.; Sopian, K. Synthesis and catalytic activity of TiO$_2$ nanoparticles for photochemical oxidation of concentrated chlorophenols under direct solar radiation. *Int. J. Electrochem. Sci.* **2012**, *7*, 4871–4888.

19. Fang, C.; Yu, R.; Liu, S.; Li, Y. Nanomaterials applied in asphalt modification: A review. *J. Mater. Sci. Technol.* **2013**, *29*, 589–594. [CrossRef]

20. Shafabakhsh, G.H.; Mirabdolazimi, S.M.; Sadeghnejad, M. Evaluation the effect of nano-TiO$_2$ on the rutting and fatigue behavior of asphalt mixtures. *Constr. Build. Mater.* **2014**, *54*, 566–571. [CrossRef]

21. Carneiro, J.O.; Azevedo, S.; Teixeira, V.; Fernandes, F.; Freitas, E.; Silva, H.M.R.D.; Oliveira, J. Development of photocatalytic asphalt mixtures by the deposition and volumetric incorporation of TiO$_2$ nanoparticles. *Constr. Build. Mater.* **2013**, *38*, 594–601. [CrossRef]

22. Nazari, H.; Naderi, K.; Nejad, F.M. Improving aging resistance and fatigue performance of asphalt binders using inorganic nanoparticles. *Constr. Build. Mater.* **2018**, *170*, 591–602. [CrossRef]

23. Zhang, H.; Zhu, C.; Yu, J.; Shi, C.; Zhang, D. Influence of surface modification on physical and ultraviolet aging resistance of bitumen containing inorganic nanoparticles. *Constr. Build. Mater.* **2015**, *98*, 735–740. [CrossRef]

24. Wang, J.; Zhang, H.; Zhu, C. Effect of multi-scale nanocomposites on performance of asphalt binder and mixture. *Constr. Build. Mater.* **2020**, *243*, 118307. [CrossRef]

25. Fan, W.; Chan, K.Y.; Zhang, C.; Leung, M.K. Advanced solar photocatalytic asphalt for removal of vehicular NOx. *Energy Procedia* **2017**, *143*, 811–816. [CrossRef]

26. Osborn, D.; Hassan, M.; Asadi, S.; White, J.R. Durability quantification of TiO$_2$ surface coating on concrete and asphalt pavements. *J. Mater. Civ. Eng.* **2014**, *26*, 331–337. [CrossRef]

27. Li, L.; Qian, C. A lab study of photo-catalytic oxidation and removal of nitrogen oxides in vehicular emissions and its fieldwork on Nanjing No. 3 bridge of Yangtze River. Technical note. *Int. J. Pavement Res. Technol.* **2009**, *2*, 218–222.

28. Hassan, M.; Mohammad, L.N.; Asadi, S.; Dylla, H.; Cooper, S., III. Sustainable photocatalytic asphalt pavements for mitigation of nitrogen oxide and sulfur dioxide vehicle emissions. *J. Mater. Civ. Eng.* **2013**, *25*, 365–371. [CrossRef]

29. Hassan, M.M.; Dylla, H.; Asadi, S.; Mohammad, L.N.; Cooper, S. Laboratory evaluation of environmental performance of photocatalytic titanium dioxide warm-mix asphalt pavements. *J. Mater. Civ. Eng.* **2012**, *24*, 599–605. [CrossRef]

30. Brovelli, C.; Crispino, M. Photocatalytic suspension for road pavements: Investigation on wearing and contaminant effects. *J. Mater. Civ. Eng.* **2013**, *25*, 548–554. [CrossRef]

31. Wang, D.; Leng, Z.; Yu, H.; Hüben, M.; Kollmann, J.; Oeser, M. Durability of epoxy-bonded TiO$_2$-modified aggregate as a photocatalytic coating layer for asphalt pavement under vehicle tire polishing. *Wear* **2017**, *382*, 1–7. [CrossRef]

32. Hassan, M.M.; Mohammad, L.N.; Cooper, S.B., III; Dylla, H. Evaluation of nano–titanium dioxide additive on asphalt binder aging properties. *Transp. Res. Rec.* **2011**, *2207*, 11–15. [CrossRef]

33. Hu, J.; Wu, S.; Liu, Q.; García Hernández, M.I.; Zeng, W.; Nie, S.; Wan, S.; Zhang, D.; Li, Y. The effect of ultraviolet radiation on bitumen aging depth. *Materials* **2018**, *11*, 747. [CrossRef] [PubMed]

34. Minero, C.; Bedini, A.; Minella, M. On the standardization of the photocatalytic gas/solid tests. *Int. J. Chem. React. Eng.* **2013**, *11*, 717–732. [CrossRef]

35. Matsuda, S.; Hatano, H. Photocatalytic removal of NOx in a circulating fluidized bed system. *Powder Technol.* **2005**, *151*, 61–67. [CrossRef]

36. Menéndez-Flores, V.M.; Bahnemann, D.W.; Ohno, T. Visible light photocatalytic activities of S-doped TiO_2-Fe^{3+} in aqueous and gas phase. *Appl. Catal. B* **2011**, *103*, 99–108. [CrossRef]

37. Kim, J.Y.; Kim, C.S.; Chang, H.K.; Kim, T.O. Effects of ZrO_2 addition on phase stability and photocatalytic activity of ZrO_2/TiO_2 nanoparticles. *Adv. Powder Technol.* **2010**, *21*, 141–144. [CrossRef]

38. Signoretto, M.; Ghedini, E.; Trevisan, V.; Bianchi, C.L.; Ongaro, M.; Cruciani, G. TiO_2–MCM-41 for the photocatalytic abatement of NOx in gas phase. *Appl. Catal. B* **2010**, *95*, 130–136. [CrossRef]

39. Lee, S.H.; Yamasue, E.; Okumura, H.; Ishihara, K.N. Effect of oxygen and nitrogen concentration of nitrogen doped TiOx film as photocatalyst prepared by reactive sputtering. *Appl. Catal. A Gen.* **2009**, *371*, 179–190. [CrossRef]

40. Bianchi, C.L.; Pirola, C.; Galli, F.; Vitali, S.; Minguzzi, A.; Stucchi, M.; Manent, F.; Capucci, V. NOx degradation in a continuous large-scale reactor using full-size industrial photocatalytic tiles. *Catal. Sci. Technol.* **2016**, *6*, 2261–2267. [CrossRef]

41. Murata, Y.; Kamitani, K.; Takeuchi, K. *Air Purifying Blocks Based on Photocatalysis*; Japan Interlocking Block Pavement Engineering Association (JIBPEA): Tokyo, Japan, 2000.

42. Guo, M.-Z.; Ling, T.-C.; Poon, C.S. Photocatalytic NOx degradation of concrete surface layers intermixed and spray-coated with nano-TiO2: Influence of experimental factors. *Cem. Concr. Compos.* **2017**, *83*, 279–289. [CrossRef]

43. Jafari, H.; Afshar, S. Improved photodegradation of organic contaminants using nano-TiO2 and TiO2–SiO2 deposited on Portland cement concrete blocks. *Photochem. Photobiol.* **2016**, *92*, 87–101. [CrossRef]

44. Noor, L.; Wasiuddin, N.M.; Mohammad, L.N.; Salomon, D. Use of Fourier Transform Infrared (FT-IR) Spectroscopy to Determine the Type and Quantity of Rejuvenator Used in Asphalt Binder. In *Recent Developments in Pavement Engineering: Proceedings of the 3rd GeoMEast International Congress and Exhibition, Egypt 2019 on Sustainable Civil Infrastructures—The Official International Congress of the Soil-Structure Interaction Group in Egypt (SSIGE)*; Springer: Berlin/Heidelberg, Germany, 2020; Volume 1, pp. 70–84.

45. Hou, X.; Lv, S.; Chen, Z.; Xiao, F. Applications of Fourier transform infrared spectroscopy technologies on asphalt materials. *Measurement* **2018**, *121*, 304–316. [CrossRef]

46. Wu, S.; Zhao, Z.; Xiao, Y.; Yi, M.; Chen, Z.; Li, M. Evaluation of mechanical properties and aging index of 10-year field aged asphalt materials. *Constr. Build. Mater.* **2017**, *155*, 1158–1167. [CrossRef]

47. Min, K.E.; Jeong, H.M. Structures and properties of semi-blown petroleum asphalt. *Appl. Chem. Eng.* **2011**, *22*, 664–671.